Carrier Localization in the Vicinity of Dislocations in InGaN

F.C-P. Massabuau,[1, a)] P. Chen,[1] M.K. Horton,[2, 3] S.L. Rhode,[3] C.X. Ren,[1] T.J. O'Hanlon,[1] A. Kovács,[4] M.J. Kappers,[1] C.J. Humphreys,[1] R.E. Dunin-Borkowski,[4] and R.A. Oliver[1]

[1)] *Department of Materials Science and Metallurgy, University of Cambridge, Cambridge, UK*

[2)] *Materials Science Division, Lawrence Berkeley National Laboratory, Berkeley, US*

[3)] *Department of Materials, Imperial College London, London, UK*

[4)] *Ernst Ruska-Centre for Microscopy and Spectroscopy with Electrons and Peter Grünberg Institute, Forschungszentrum Jülich GmbH, Jülich, Germany*

(Dated: 21 November 2016)

We present a multi-microscopy study of dislocations in InGaN, whereby the same threading dislocation was observed under several microscopes (atomic force microscopy, scanning electron microscopy, cathodoluminescence imaging and spectroscopy, transmission electron microscopy), and its morphological optical and structural properties directly correlated. We achieved this across an ensemble of defects large enough to be statistically significant. Our results provide evidence that carrier localization occurs in the direct vicinity of the dislocation through the enhanced formation of In-N chains and atomic condensates, thus limiting non-radiative recombination of carriers at the dislocation core. We highlight that the localization properties in the vicinity of threading dislocations arise as a consequence of the strain field of the individual dislocation and the additional strain field building between interacting neighboring dislocations. Our study therefore suggests that careful strain and dislocation distribution engineering may further improve the resilience of InGaN-based devices to threading dislocations. Besides providing a new understanding of dislocations in InGaN, this paper presents a proof-of-concept for a methodology which is relevant to many problems in materials science.

[a]fm350@cam.ac.uk

I. INTRODUCTION

Owing to a direct band gap ranging from the ultraviolet ($E_{g\,GaN} = 3.51$ eV) to the infrared ($E_{g\,InN} = 0.7$ eV)[1], $In_xGa_{1-x}N$ (which for convenience we abbreviate to InGaN) has become the leading semiconductor for numerous optoelectronic applications. Whilst thin layers of InGaN (thickness below $\sim$5 nm) are employed in the active region of light emitting diodes (LEDs), as quantum wells (QWs)[2,3], thick layers of InGaN (thickness above 20 nm) find application as the active region in solar cells[4–7], as prelayers located under the InGaN/GaN QW stack in LEDs[8–10] or as sacrificial layers for example in the fabrication of microdisk[11] or nanobeam[12] lasers.

However this material is characterized by a high density of threading dislocations, which are commonly associated with non-radiative recombination centers[13–17]. Threading dislocations in InGaN fall into three categories depending on their Burgers vector, $\mathbf{b}$, namely edge-type ($\mathbf{b} = \mathbf{a}$), mixed-type ($\mathbf{b} = \mathbf{a} + \mathbf{c}$) and screw-type ($\mathbf{b} = \mathbf{c}$) dislocations, and have been reported to be terminated by V-shaped pits[18]. However InGaN-based devices are surprisingly resilient to the presence of such high densities of threading dislocations. Several mechanisms have been suggested to explain this resilience[19] but the role of dislocations in InGaN is still ambiguous and poorly understood.

In this study we observed the same threading dislocation in a thick layer of InGaN under different microscopes, namely atomic force microscopy (AFM), scanning electron microscopy (SEM), cathodoluminescence (CL) and transmission electron microscopy (TEM). This approach, referred to as "multi-microscopy"[20], allowed us to directly correlate the morphological, optical and structural properties of that specific dislocation. We observed an enhancement of the CL emission at the center of the V-pits, which could be ascribed to an enhanced formation of In-N chains and atomic condensates and localize carriers in the vicinity of the dislocation core. The correlation of these multiple microscopy techniques allowed us to link the carrier localization properties to the strain of the individual dislocation as well as to that arising from the interaction of neighboring dislocations, while showing no measurable impact of the core structure of the dislocation itself.

II. EXPERIMENTAL METHODS

A. Sample Growth and Characterization

A Si-doped InGaN epilayer was grown by metal-organic vapor phase epitaxy (MOVPE) in a Thomas Swan 6 × 2 inch close-coupled showerhead reactor. Trimethylgallium (TMG), trimethylindium (TMI), diluted silane in hydrogen (SiH$_4$) and ammonia (NH$_3$) were used as precursors for the Ga, In, Si and N elements, respectively. Hydrogen (H$_2$) was used as the carrier gas for the growth of GaN, while a mixture of hydrogen and nitrogen (N$_2$) was employed for InGaN growth. Pseudo-substrates consisting of *ca.* 5 μm of GaN (of which 2 μm undoped and 3 μm Si-doped to 5×10^{18} cm^{-3}) grown on c-plane sapphire with a miscut of $0.25 \pm 0.10°$ towards (11$\bar{2}$0) were employed, yielding a threading dislocation density of 4×10^8 cm^{-2} approximately. After the growth of a 500 nm thick GaN connecting layer, the InGaN layer was grown at 749°C using a TMI flow of 8.1 μmol.min^{-1}, a TMG flow of 5.9 μmol.min^{-1}, a SiH$_4$ flow of 0.6 nmol.min^{-1} resulting in a Si-doping of approximately 5×10^{18} cm^{-3}, a NH$_3$ flow of 446 mmol.min^{-1}, and a H$_2$ flow rate of 200 sccm (standard cubic centimetre per minute) to improve the surface quality[21]. The thickness and composition of the InGaN layer were obtained by X-ray diffraction (XRD) on a Philips X-pert MRD diffractometer, using a four-bounce Ge(220) monochromator and a three-bounce Ge(220) analyzer crystal. Analysis of the symmetric 002 reflection yields a thickness of the InGaN layer of 136 ± 2 nm and an indium composition of $x = 8.6 \pm 0.5\%$. Reciprocal space maps taken around the symmetric 006 and asymmetric 204 reflections revealed that the InGaN layer is fully strained on the GaN pseudo-substrate. The sample was prepared for multi-microscopy analysis using the set-up described in earlier work[20], consisting of a copper grid, as is used in TEM sample preparation, positioned at the surface of the sample. Using the 50 μm size square mesh as well as the trench defects at the surface of the sample (basal plane stacking fault bounded by a vertical stacking mismatch boundary which opens up at the sample surface as a trench enclosing a region of material)[22–24], the same V-defects could be easily identified in the different microscopes: AFM, SEM, CL and high angle annular dark-field scanning TEM (HAADF-STEM). About 600 dislocations have been analyzed by AFM and SEM-CL, and about 30 of them have been observed at the atomic scale by TEM. It should be mentioned that the experiment was conducted in the following order: AFM,

SEM-CL, TEM sample preparation, TEM.

B. Analysis of AFM data

AFM, performed on a Veeco Dimension 3100 operating in tapping mode, was used to determine the dislocation type and the distance to nearest neighbor of each of the 600 dislocations. In III-Nitrides, threading dislocations have their line direction parallel to [0001] and fall into in three categories depending on their Burgers vector. Therefore a-type, c-type and a+c-type dislocations - respectively edge, screw and mixed-type dislocations - have a Burgers vector $\mathbf{b} = 1/3 \langle 11\bar{2}0 \rangle$, $\mathbf{b} = [0001]$ and $\mathbf{b} = 1/3 \langle 11\bar{2}3 \rangle$, respectively[25]. The dislocation type can be determined by AFM using the diameter of the V-pit which terminates the dislocation[26]. The diameter of the V-defects was measured as the distance between the two sides of the pit taken 4 nm below the average level of the surrounding material. It is worth noting that in order to reduce the impact of the tip status on our measurements, all the AFM images were taken using the same fresh tip. Using this method, two distinct populations of V-defects can be directly identified, one type of pits of smaller diameter identified as V-pits originating from edge-type dislocations and the other type of larger diameter corresponding to mixed-type dislocations. Finally a third group can be observed, with a diameter greater than that of the other two populations, and relates to V-pits originating from screw-type dislocations. The ratio of edge, mixed and screw-type dislocations is 55%, 45% and <1%, respectively, in agreement with results from studies carried out on similar pseudo-substrates[26,27]. It should be noted that only 2 out of the 600 dislocations are of pure screw character, and therefore are not discussed here due to their poor statistical relevance.

C. Analysis of SEM-CL data

SEM-CL was conducted at room temperature using an FEI field emission gun XL30 SEM, and coupled with a Gatan MonoCL4 CL system. The spatial resolution of CL measurements is a function of several factors (including probe size, interaction volume size, and carrier diffusion length) but is primarily determined by the size of the interaction volume[28]. The SEM was operated at 3 kV, hence the interaction volume is $R_{KO} = 120$ nm approximately[29].

This results in the CL signal to originate from $0.3\,R_{KO} \sim$ 30-40 nm below the surface[30] (which corresponds to the depth at which the electron energy-loss profile reaches a maximum). Taking into account the absorption of an emitted photon by the material (which is generally quite high for III-Nitrides, with a typical absorption coefficient of $\sim 10^5$ cm^{-1})[31], the majority of the CL signal collected must arise from the first 25-30 nm of material below the surface. This value was confirmed using a Monte Carlo simulation[32]. The slits and diffraction grating of the CL system were set at 0.2 mm and 1200 lines/mm, respectively, thus allowing a 0.5 nm spectral resolution. The light emission was recorded between 370 nm to 430 nm approximately, with the peak emission of the sample being at 406 nm. For each of the V-pits previously observed by AFM, a series of CL emission spectra were recorded along a line scan crossing the V-pit, about 500 nm long and with a pitch of 25 nm approximately (*i.e.* comparable to the lateral size of the interaction volume). For each line spectra across a V-pit, the data analysis was performed as follows. Each spectrum was first fitted using a single Gaussian function. The central wavelength and intensity of the Gaussian fits were then recorded and plotted as a function of the probe position. The pixels allocated to the V-pit were firstly identified and then the remaining pixels - allocated to the surrounding material only - were fitted by a third order polynomial function. This allowed us to fit the variations in intensity and peak emission wavelength of the material surrounding the V-pit. (Given that the intensity and peak emission of the surrounding material, non-affected by the presence of V-pits, is not uniform across the sample, for example because of the presence of compositional or strain fluctuations, additional line spectra similar in length and pixel size were recorded on regions unaffected by the V-pits. This allowed the determination of the best fit for the fluctuations in wavelength and intensity of the material surrounding the V-pits, showing the third-order polynomial to be the most suitable approach.) The data thus recorded to characterize each V-pit are the "energy shift", measured as the difference in emission energy between the experimental data and the "surrounding" polynomial fit taken at the position of the center of the pit, and on the facets of the pit, and the "intensity ratio", measured as the ratio between the intensity of the experimental data and the "surrounding" polynomial fit at the position of the center of the pit, and on the facets of the pit.

D. Analysis of TEM data

The sample was prepared for plan-view imaging in the TEM using standard mechanical polishing method followed by Ar^+ ion milling at 5 kV and cleaning at 1 kV. Finally, acetone and a dilute solution of nitric acid were used to clean the sample from thermal wax and from sputtering of material back to the TEM foil during the ion milling process. HAADF-STEM was performed on an FEI Titan G2 80-200 with a detector collection semi-angle of 69 mrad. In order to prevent electron beam damage in the TEM[33,34], the microscope was operated at 80 kV, which is below the knock-on threshold for InGaN[34]. The threading dislocations could be easily identified in ADF-STEM contrast due to the foil thickness reduction induced by the presence of a V-pit at their termination, resulting in a sudden change in contrast. The dislocations were observed along the [0001] zone-axis (*i.e.* parallel to the dislocations line direction), thus allowing identification of the core structure[27,35].

III. RESULTS AND DISCUSSION

A. Multi-microscopy proof-of-concept

Figure 1 gives an example of multi-microscopy observation of dislocations in InGaN which demonstrates the ability to perform a one-to-one analysis of the same threading dislocations by AFM, SEM, CL and TEM. In several cases the dislocations have been observed at the atomic scale, where the core structure as well as the strain domains around the dislocation could be identified (Figure 1(e)-(f)). It should be noted that the GPA is used here only qualitavely, as an illustration of the regions of tensile and compressive strain around the dislocation core. One can see that the V-pits, directly observable on the AFM and SEM pictures (Figure 1(a)-(b)), coincide with bright spots surrounded by a darker halo in the CL image (Figure 1(c)). This observation indicates enhanced light emission properties from the central part of the V-pit, where the dislocation is located, in contrast to previous reports which only observed dark spots by CL and therefore concluded that dislocations are non-radiative recombination centers[13–15].

The correlation between the AFM measurements (which give "dislocation type", *i.e.* edge-, mixed- or screw-type, and "distance to nearest neighbor", *i.e.* smallest distance between the center of the V-pit of interest and that of the surrounding V-pits), and the
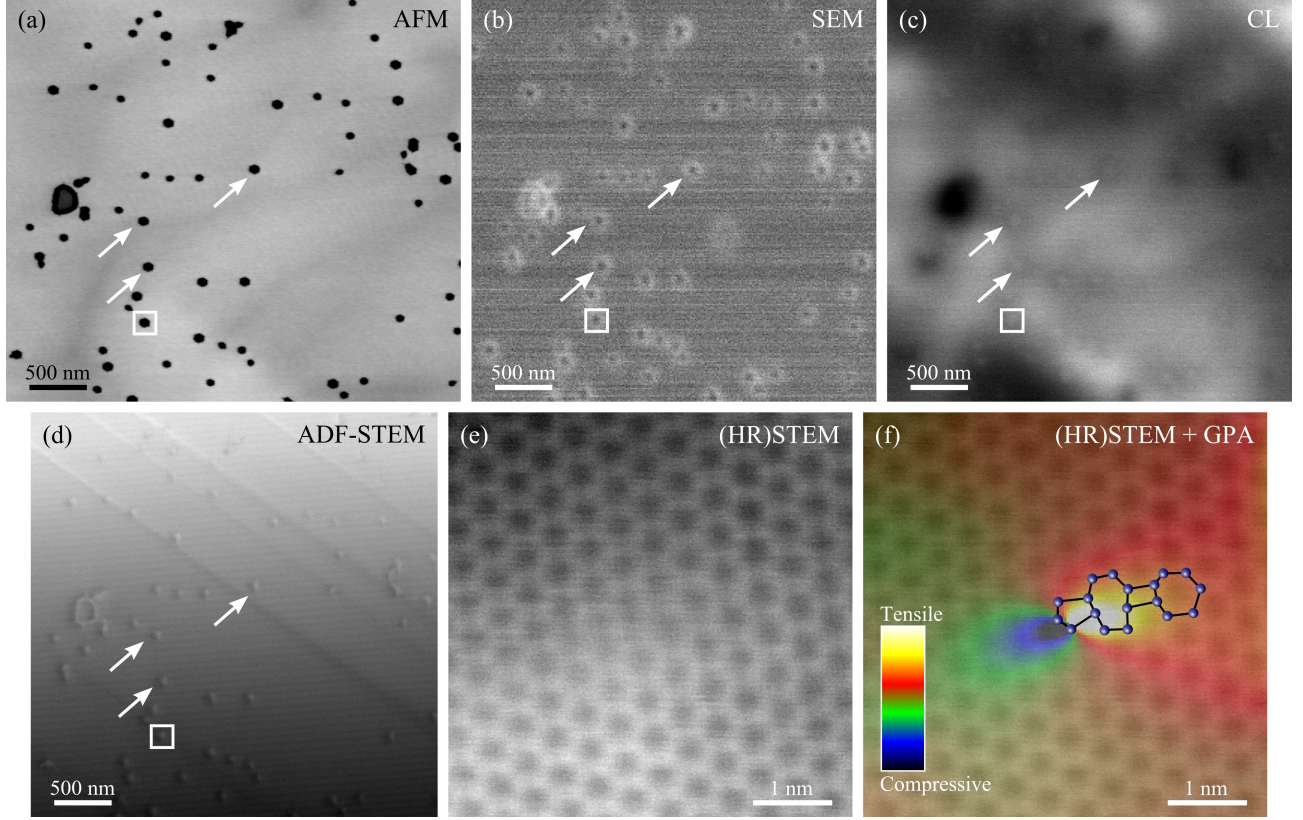
7

FIG. 1. AFM (a), SEM (b), panchromatic CL (c), and ADF-STEM (d) performed on the same micrometre-scale area. To guide the eye, a few dislocations are indicated by arrows in each picture. (e) High-resolution (HR) STEM image of the dislocation indicated by a square in (a)-(d), enabling the identification of the core structure (here dissociated 7/4/8/5-atom ring), and (f) geometric phase analysis (GPA) showing the ϵ_{xx} strain component of the dislocation core region.

SEM-CL measurements ("intensity ratio" and "energy shift" from different parts of the V-pit, *i.e.* emission intensity and energy relative to the surrounding material) is illustrated in Figure 2. (It should be noted that no correlation was found between the diameter of the V-pit and the emission properties recorded at the center of the V-pit (yellow region in Figure 2) or from its facet (green region in Figure 2), hence we believe that the results we present here are not an artefact due to a difference in light extraction efficiency between the V-pit and its surroundings. Additionally, the fact that both energy shift and intensity ratio depend on nearest neighbor distance also indicates that this is not an extraction efficiency effect, since roughening induced increases in extraction efficiency do not lead to energy shifts.) Irrespective of the position of the probe and of the dislocation type, both the intensity
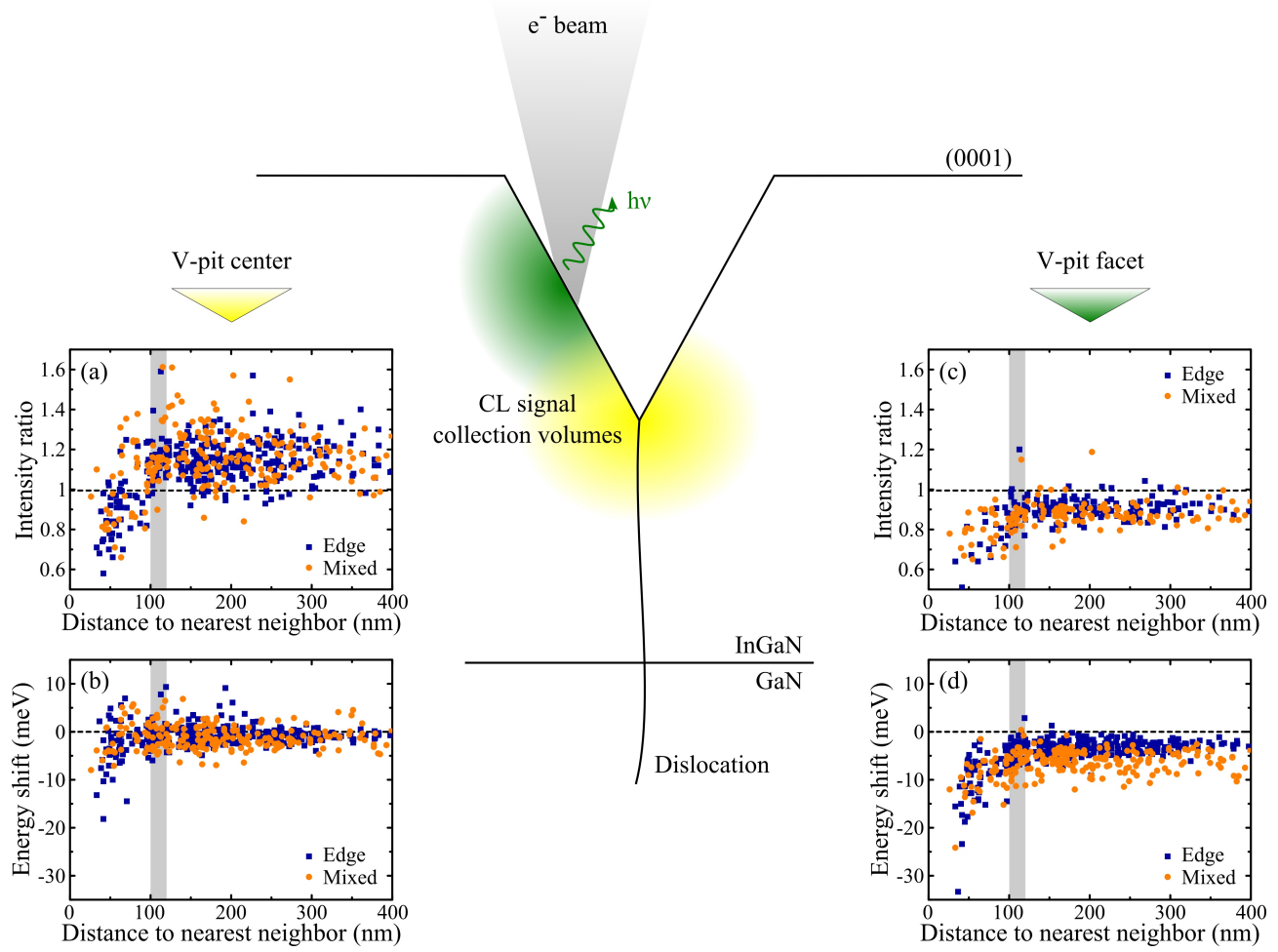
FIG. 2. Schematic showing the electron probe in the SEM-CL scanning across a V-pit. The scale of the schematic, although indicative, is representative of the experimental conditions in which the experiment was conducted. Distance to nearest neighbor dependence of the intensity ratio (a)(c) and energy shift (b)(d) measured at the center (a)(b) and facet (c)(d) of the V-pits.

ratio and energy shift can be observed to increase as the distance to nearest neighboring dislocation increases before reaching a plateau. In all the graphs the transition between the two regimes occurs for dislocation separations of 100-120 nm, as indicated by the grey bars in Figure 2. For convenience we will refer to the threading dislocations with spacing below 100 nm as "clustered dislocations", and to those with spacing above 120 nm as "isolated dislocations".

B. Investigation of isolated dislocations

Looking in more detail at the properties of isolated dislocations, it can be seen that the intensity ratio measured in the center of the V-pit (*i.e.* in the close vicinity of the dislocation core) is above unity (Figure 2(a)), which is in line with the enhanced luminescence shown in Figure 1(c). On average, the emission intensity is increased by 15% with a standard deviation $\sigma = 10\%$ for isolated edge-type dislocations, and by 17% ($\sigma = 13\%$) for isolated mixed-type dislocations. (Note that the standard error here is under 1%, but standard deviations are quoted to indicate the width of the distribution). This result suggests an increase in the radiative recombination rate occurring in the vicinity of the dislocation core. It can also be noted that the energy shift remains close to zero (Figure 2(b)). The shift from the center of the V-pit is -1 meV ($\sigma = 2$ meV) for isolated edge-type dislocations, with minimum and maximum values of -5 meV and +9 meV, respectively. For isolated mixed-type dislocations this shift is -1 meV ($\sigma = 2$ meV) with minimum and maximum values of -7 meV and +7 meV, respectively. On the other hand, on the facets of the V-pit the intensity ratio remains below unity (Figure 2(c)) whereby we note a reduction of the CL emission by 9% ($\sigma = 4\%$) for isolated edge-type dislocations and 11% ($\sigma = 6\%$) for isolated mixed-type dislocations. The energy shift is almost always observed to be negative (*i.e.* emission redshifted compared to the surrounding material), -3 meV ($\sigma = 1$ meV) for edge-type dislocations with minimum and maximum values of -9 meV and +1 meV, respectively. For mixed-type dislocations the shift is -6 meV ($\sigma = 2$ meV) with minimum and maximum values -12 meV and -1 meV, respectively (Figure 2(d)). It is worth pointing out that except in the case of the energy shift measured on the facets, the optical properties have no measureable dependence on the dislocation type. It can then be inferred that the mechanism explaining the emission properties of the dislocation itself is distinct from that determining the properties of the facets of the V-pit which forms at its apex. Given the local character of the properties we report (*i.e.* variations on a lateral scale of a few nms), as well as the energy shifts involved in this experiment (*i.e.* a few meVs), two main mechanisms can be considered: strain relaxation[36,37] and formation of In-N chains and atomic condensates[38–40] (in short "In-N chains").

Using XRD the InGaN layer was found to be, on average, fully strained on the GaN pseudo-substrate (within experimental accuracy of 3%). However the presence of a threading

dislocation disturbs the strain state locally. Indeed the dislocation is bordered by a region of higher strain - *i.e.* compressive region - and a region of lower strain - *i.e.* tensile region - as illustrated in Figure 1(f). Additionally, dislocations in InGaN form V-pits as a means to reduce the strain in the material[36], thus leading to a local strain relaxation around the facets of the V-pit. A variation in strain commonly induces a variation in the transition energy in the material. Indeed a recent study performed on a number of thick InGaN films reported that the band gap bowing parameter varied as a function of the relaxation[37]. Based on the values of bowing reported in this study, a full relaxation of the InGaN would induce a decrease in the emission energy of 129 meV in our sample. Hence a (local) partial relaxation of the material could lead to a redshift of the CL emission similar to what we report. It is worth noting that we do not ascribe the CL emission properties to a different indium incorporation on the facets of the V-pit as compared to the surrounding material because the energy shift is observed to vary with dislocation type, which cannot be easily explained by mechanisms other than strain relaxation. Besides, the compositional variations required to cause such low energy shifts must be $\ll 1\%$. Therefore, we attribute the emission properties of the facet of the V-pit, whereby the emission intensity is poorer than that of the surrounding material, and the energy shift is almost systematically negative and dependent on the dislocation type, to strain relaxation occurring on the facets of the V-pit. The intensity ratio below unity could be explained by a lesser amount of localization centers in this region, thus leading to a fraction of the carriers to recombine non-radiatively at the dislocations core.

The presence of In-N chains in the material has been found, theoretically[38,39] and experimentally[40], to strongly localize holes in InGaN. Using a first-principle density functional theory approach on $In_{0.14}Ga_{0.86}N$ alloy, Liu *et al.* predicted that the formation of In-N zigzag chains and In-N atomic condensates localized the valence band states and reduced the energy band gap by 20 meV and 100 meV, respectively[38]. Similarly, Schulz *et al.* used density functional theory calculations on dilute InGaN alloys to determine the effect of having one to four indium atoms sharing a same nitrogen atom on carrier localization[39]. Their results revealed a strong hole wavefunction localization associated by a decrease of the band gap energy. Compared to a single In-N bond, an In-N chain (*i.e.* two or more indium atoms sharing a same nitrogen atom) were found to decrease the band gap energy by 8 meV (two indium atoms), 18 meV (three indium atoms), and 29 meV (four indium atoms).

Moreover, the excited hole states were localized up to 50 meV from the valence band edge. Thus an In-N chain or atomic condensate would localize the holes while inducing an energy shift between approximately +42 meV and -8 meV (two indium atoms), +32 meV and -18 meV (three indium atoms), and +21 meV and -29 meV (four indium atoms). Moreover, recent studies reported that indium tends to segregate in the tensile part of the core of threading dislocations in thick InGaN layers[35,41]. Our data then suggest that the enhanced emission recorded in the center of the V-pit, and the low energy shift independent of the dislocation type are ascribed to an increase in the number of In-N chains forming in the vicinity of the dislocation core as a result of the indium segregation reported by Horton *et al.* and Rhode *et al.*[35,41]. It should be noted that the segregation of indium atoms at the vicinity of the dislocation core was reported to occur within a few nanometers from the core of the dislocation, and hence does not alter our measurements and conclusions reported on the V-pit facets.

To investigate this hypothesis further, Metropolis Monte Carlo simulations of indium segregation to a dislocation core were performed to obtain statistical information on the expected length and distribution of In-N chains if indium segregation occurs relative to that of a random alloy. To match our sample, the calculation considered a volume of InGaN of composition 8.6% strained to match a GaN template and containing an edge-type dislocation. The 5/7-atom ring edge-type core was selected as a representative example, since there are too many unique core structures in the wurtzite crystal system to do a systematic analysis of all core types. However, since segregation of comparable magnitudes is expected for all core types[41], this example should prove sufficient. The dimensions of the supercell are 64a × 64a × 16c, with Monte Carlo swaps performed in the vicinity of a single dislocation core. Equilibrium was said to be obtained after approximately 6×10^4 trial swaps when the trend in total potential energy stops decreasing and instead fluctuates around a constant level and the local concentration around the dislocation core stabilized, although a total of 1.8×10^5 trial swaps were ultimately performed. Further details on this computational methodology can be found detailed elsewhere[41]. Graph-tool[42] was used to extract additional information from the resulting microstructure. Histograms of the results are shown in Figure 3, obtained by counting the number and length of In-N chains within a cylinder of radius 10 Å centered on the dislocation core. Alongside the histogram are 2D abstract illustrations of the crystal graph whereby each point represents an In atom, and a
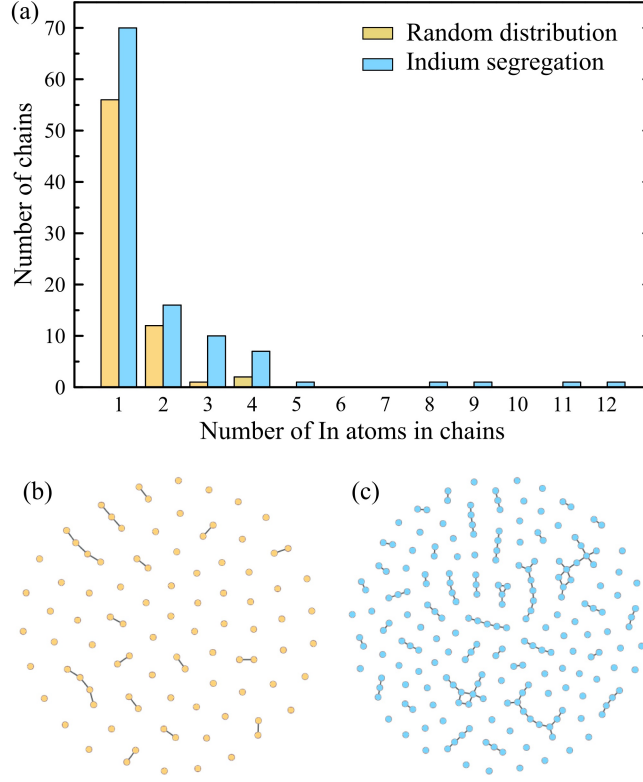
FIG. 3. (a) Histogram of the number of In-N chains as a function of the number of indium atoms in the chains, located within a 10 Å radius centered on the dislocation, in the case of a random distribution of indium (*i.e.* initial configuration of the simulation) or segregation of indium (*i.e.* equilibrium configuration of the simulation). Abstract representation of the data in (a), in the case of a random distribution (b) or segregation (c) of indium atoms.

point joined to another point represents an In-N-In chain (Figure 3(b) - random alloy,(c) - indium segregation to dislocation core). At equilibrium, a significantly higher proportion of longer chains can be clearly seen, and in particular a significant proportion of 3-In-containing and 4-In-containing chains, which would be comparatively rare in a random alloy at this composition. These results support the proposition that the enhanced emission properties measured in the center of the V-pit arise from the formation of In-N chains in the vicinity of the dislocation core.
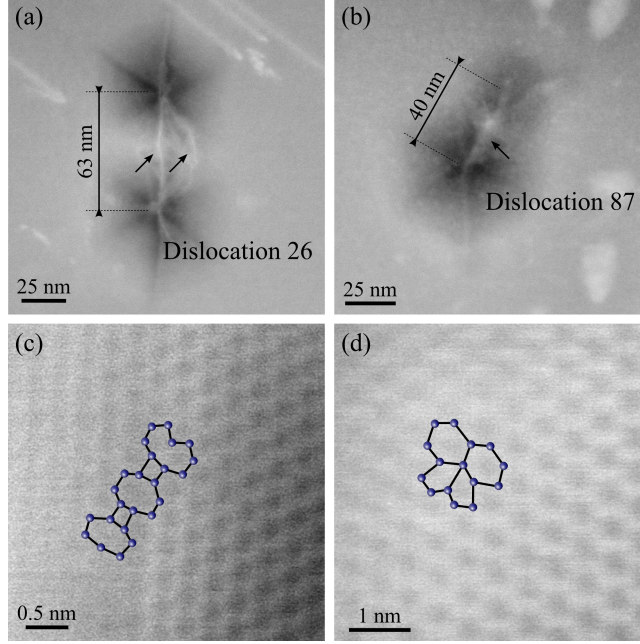
FIG. 4. ADF-STEM image of the clustered dislocations 26 (a) and 87 (b). The white strain-related contrast between the neighboring dislocations is indicated by an arrow. Aberration-corrected HAADF-STEM image of the core of dislocation 26 (dissociated 7/4/8/4/9-atom ring)(c) and 87 (undissociated double 5/6-atom ring)(d). An ABSF-filter (Average Background Subtraction Filter) has been applied to (c) and (d) in order to remove noise from the images.

C.   Investigation of clustered dislocations

Figure 2 highlighted different emission properties for those threading dislocations which have a distance to their nearest neighbor below 100-120 nm - *i.e.* clustered dislocations. In this configuration, both the intensity ratio and energy shift were observed to decrease when the dislocation is closer to its neighbor. For the dataset recorded on the center of the V-pit, we note a sharp decrease in the intensity ratio down to below unity. Similarly, we record increasing negative energy shifts, down to -18 meV. For the data taken on the facet of the V-pit, this phenomenon is even more pronounced with lower intensity ratios and energy shifts down to -33 meV. Based on our earlier arguments, these observations can be attributed to a decrease in strain affecting the V-pit globally (facet and center). We tentatively attribute that decrease in strain to the additional strain field that is generated when two neighboring dislocations are close enough to interact with each other. The intensity ratio is reduced in clustered dislocations, perhaps as a consequence of having an additional non-radiative center

14

- *i.e.* the neighboring dislocation - within the CL generation volume. Figure 4 shows ADF-STEM images of two clustered mixed-type dislocations (referred to as "Dislocation 26" and "Dislocation 87"). Dislocations 26 and 87 are representative of typical clustered dislocations having distances to nearest neighbors of 63 nm and 40 nm respectively, intensity ratios in the center of the V-pit of 0.66 and 0.81 respectively, and energy shifts in the center of the V-pit of -4 meV and -6 meV respectively. Figure 4(a),(b) highlights the interaction of these two dislocations with their neighbor. ADF-STEM is an imaging technique which is generally used for Z-contrast imaging, although the contrast is also sensitive to the strain and to the foil thickness. A bright contrast (indicated by arrows in Figure 4(a),(b)) can be clearly observed linking the apices of the two neighboring dislocations, which indicates a change in strain in the region between the two dislocations compared to the surrounding material. The geometry of this contrast makes it very unlikely to be Z-related (*i.e.* indicating an increase in indium composition), and furthermore the required compositional variation to achieve such a contrast change would incur a much larger energy shift than that which is observed. Therefore Figure 4 further confirms that the CL emission properties of clustered dislocations arise from the additional strain relaxation mechanism due to the proximity of two (or more) dislocations.

Figure 4 also shows the dislocation core structures of Dislocations 26 (Figure 4(c)) and 87 (Figure 4(d)). It reveals that whilst Dislocation 26 has a dissociated core, with formation of a 7/4/8/4/9-atom ring, the core of Dislocation 87 is undissociated, with a double 5/6-atom ring[27,35]. Despite being both mixed-type, these two dislocations exhibit a fundamentally different core property in which the core of Dislocation 26 dissociated in order to reduce its energy (through formation of two partial dislocations and a stacking fault)[43] while Dislocation 87 did not. One might have suggested that the dislocation's core structure may influence the emission properties of the material in its vicinity. However we saw that the CL emission properties are quite similar between these two dislocations, therefore indicating that the impact of the core structure on the optical properties of a dislocation is negligible. The fact that edge-type dislocations only take one specific core configuration in our sample (we only observed 5/7-atom ring cores, in agreement with Rhode *et al.*)[27,35], irrespective of the isolated or clustered configuration, but exhibit the same variations in emission properties as the mixed-type dislocations further validates this point.
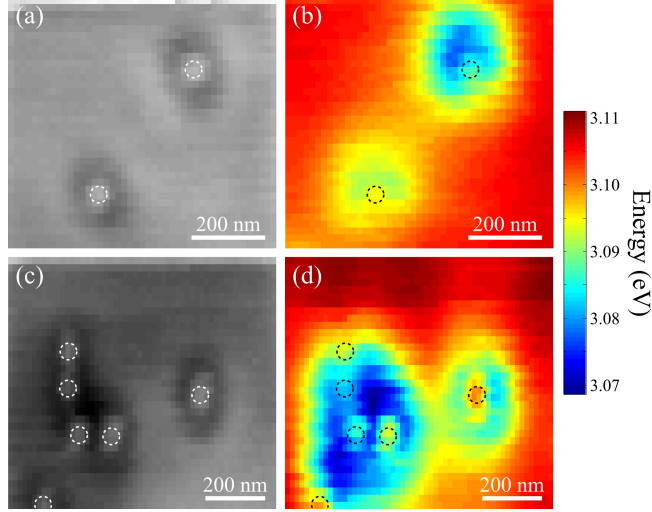
FIG. 5. 16K CL integrated intensity (a)(c) and peak emission energy (b)(d) maps of isolated (a)(b) and clustered (c)(d) dislocations. To guide the eye, the position of the bright spots, directly observable in (a) and (c), is indicated by circles in all the maps. To emphasize the relative variations in intensity and energy between isolated and clustered configurations, a common color scale is used in (a) and (c) and in (b) and (d).

D. Comparison with liquid He SEM-CL

In order to consolidate our analysis, the sample has been observed by CL in the SEM at a temperature of 16K. Decreasing the temperature has many advantages; in particular it leads to a decrease of the non-radiative recombination rate in the material resulting in a dramatic increase of the CL signal. This consequently enables us to record spectral maps (instead of spectral lines) with improved spectral resolution (herein 0.2 nm approximately). Figure 5 shows an example of such maps taken around isolated (Figure 5(a)-(b)) and clustered (Figure 5(c)-(d)) dislocations, and which qualitatively summarizes and corroborates the measurements reported in Figure 2.

The intensity maps in Figure 5(a),(c) clearly show the presence of a bright spot surrounded by a darker halo at the position of a dislocation, which supports our observations made by room temperature CL as well as the measurements of intensity ratio reported earlier. The bright spot and the dark halo can be also easily distinguished in the energy map as their energy domains are distinct. The bright spot - corresponding to the emission from the center of the V-pit - exhibits a weak redshift of its emission energy relative to the sur-

rounding material, as was shown quantitatively in Figure 2(b). In comparison the shift in energy measured on the facets of the V-pits - the dark halo - is much greater, in line with the results reported in Figure 2(d). While the emission properties from the center of the V-pit have been ascribed to the enhanced formation of In-N chains in the tensile region of the dislocation core, those from the facet of the V-pit have been attributed to strain relaxation. The possibility of recording CL maps highlights a very interesting feature which supports this analysis. In Figure 5(b) it can be seen that although a low energy ring surrounds the position of the dislocations (indicated by a circle), one side of the ring has a significantly more pronounced energy shift, making the ring appear like a bean partially encircling the dislocation. This asymmetry is the emission energy signature of the tensile (low energy side of the ring) and compressive (high energy side of the ring) regions of the dislocation superimposed on the strain relaxation from the V-pit facets. Finally Figure 5(c)-(d) show the intensity and emission energy maps recorded around clustered dislocations. Facilitated by the use of a common color scale with Figure 5(a)-(b), it can be seen that, similar to what was reported in Figure 2, the intensity ratio is decreased and the energy shift is more pronounced compared to the configuration where the dislocations are isolated. It can be noted that the low energy domain that in the isolated dislocation case we noted was asymmetric and bean-shaped, is now much larger and links all the dislocations in the cluster. This corroborates our earlier observations that the stronger energy shift in clustered dislocations relates to additional strain relaxation arising from the proximity of the dislocations.

This experiment corroborates our quantitative analysis described in sections A-C. It also further supports that the phenomena we observed are not due to a light extraction effect because the relative position of the bright spot to the dark halo - as well as their energy counterparts - varies between dislocations; the bright spot is sometimes centered on the halo, but very often off-centered in various different directions. Were this a light extraction effect, we would expect it to occur similarly for all isolated dislocations since the pit shapes vary very little.

IV. CONCLUSION

In conclusion we conducted a multi-microscopy analysis of a statistically significant number of dislocations in InGaN where we achieved the observation of each of these nanometer-

scale defects in several microscopes. Enhanced luminescence was observed by CL in the central part of the V-pits. Our data support the hypothesis that carrier localization occurs in the vicinity of dislocations in InGaN through formation of In-N chains and atomic condensates, as a consequence of indium segregating at the tensile region of the dislocation core. In the specific case of clustered dislocations, different optical properties were observed which we attribute to an additional strain relaxation due to the proximity of the dislocations which tends to screen the effects of the carrier localization. We show that the core structure of the dislocation has no impact on its emission properties. Instead, our results indicate that the key to the optical properties of dislocations lies in the strain field of each dislocation and the strain field building between neighboring dislocations. Our study therefore suggests that the spatial distribution of dislocations may have more impact on the emission properties of InGaN alloys than their actual density, and that careful strain and dislocation distribution engineering may further improve the resilience of InGaN-based devices to threading dislocations.

ACKNOWLEDGMENTS

REFERENCES

[1]I. Vurgaftman and J. R. Meyer, "Band parameters for nitrogen-containing semiconductors," Journal of Applied Physics **94**, 3675 (2003).

[2]C. Humphreys, "Solid-State Lighting," MRS Bulletin **33**, 459 (2008).

[3] M. Krames, O. Shchekin, R. Mueller-Mach, G. Mueller, L. Zhou, G. Harbers, and M. Craford, "Status and Future of High-Power Light-Emitting Diodes for Solid-State Lighting," Journal of Display Technology **3**, 160 (2007).

[4] C. Neufeld, N. Toledo, S. Cruz, M. Iza, S. DenBaars, and U. Mishra, "High quantum efficiency ingan/gan solar cells with 2.95 ev band gap," Applied Physics Letters **93**, 143502 (2008).

[5] Y. Zhang, M. Kappers, D. Zhu, F. Oehler, F. Gao, and C. Humphreys, "The effect of dislocations on the efficiency of InGaN/GaN solar cells," Solar Energy Materials and Solar Cells **117**, 279 (2013).

[6] X. Cai, S. Zeng, and B. Zhang, "Fabrication and characterization of InGaN p-i-n homojunction solar cell," Applied Physics Letters **95**, 2007 (2009).

[7] E. Matioli and C. Weisbuch, "Direct measurement of internal quantum efficiency in light emitting diodes under electrical injection," Journal of Applied Physics **109**, 073114 (2011).

[8] T. Akasaka, H. Gotoh, T. Saito, and T. Makimoto, "High luminescent efficiency of InGaN multiple quantum wells grown on InGaN underlying layers," Applied Physics Letters **85**, 3089 (2004).

[9] P. Törmä, O. Svensk, M. Ali, S. Suihkonen, M. Sopanen, M. Odnoblyudov, and V. Bougrov, "Effect of InGaN underneath layer on MOVPE-grown InGaN/GaN blue LEDs," Journal of Crystal Growth **310**, 5162 (2008).

[10] M. J. Davies, P. Dawson, F. C. Massabuau, R. A. Oliver, M. J. Kappers, and C. J. Humphreys, "The effects of Si-doped prelayers on the optical properties of InGaN/GaN single quantum well structures," Applied Physics Letters **105**, 092106 (2014).

[11] I. Aharonovich, A. Woolf, K. Russell, T. Zhu, N. Niu, M. Kappers, R. Oliver, and E. Hu, "Low threshold, room-temperature microdisk lasers in the blue spectral range," Applied Physics Letters **103**, 021112 (2013).

[12] N. Niu, A. Woolf, D. Wang, T. Zhu, Q. Quan, R. Oliver, and E. Hu, "Ultra-low threshold gallium nitride photonic crystal nanobeam laser," Applied Physics Letters **106**, 231104 (2015).

[13] T. Sugahara, H. Sato, M. Hao, Y. Naoi, S. Kurai, and S. Tottori, "Direct evidence that dislocations are non-radiative recombination centers in gan," Japanese Journal of Applied Physics **37**, 398 (1998).

[14]S. Rosner, E. Carr, M. Ludowise, G. Girolami, and H. Erikson, "Correlation of cathodoluminescence inhomogeneity with microstructural defects in epitaxial gan grown by metalorganic chemical-vapor deposition," Applied Physics Letters **70**, 420 (1997).

[15]D. Cherns, S. Henley, and F. Ponce, "Edge and screw dislocations as nonradiative centers in InGaN/GaN quantum well luminescence," Applied Physics Letters **78**, 2691 (2001).

[16]Q. Dai, M. Schubert, M. Kim, J. Kim, E. Schubert, D. Koleske, M. Crawford, S. Lee, A. Fischer, G. Thaler, and M. Banas, "Internal quantum efficiency and nonradiative recombination coefficient of GaInN/GaN multiple quantum wells with different dislocation densities," Applied Physics Letters **94**, 111109 (2009).

[17]A. Armstrong, T. Henry, D. Koleske, M. Crawford, K. Westlake, and S. Lee, "Dependence of radiative efficiency and deep level defect incorporation on threading dislocation density for InGaN/GaN light emitting diodes," Applied Physics Letters **101**, 162102 (2012).

[18]N. Sharma, P. Thomas, D. Tricker, and C. Humphreys, "Chemical mapping and formation of V-defects in InGaN multiple quantum wells," Applied Physics Letters **77**, 1274 (2000).

[19]R. Oliver, S. Bennett, T. Zhu, D. Beesley, M. Kappers, D. Saxey, A. Cerezo, and C. Humphreys, "Microstructural origins of localization in InGaN quantum wells," Journal of Physics D: Applied Physics **43**, 354003 (2010).

[20]F. Massabuau, L. Trinh-Xuan, D. Lodie, E. Thrush, D. Zhu, F. Oehler, T. Zhu, M. Kappers, C. Humphreys, and R. Oliver, "Correlations between the morphology and emission properties of trench defects in InGaN/GaN quantum wells," Journal of Applied Physics **113**, 073505 (2013).

[21]E. Taylor, F. Fang, F. Oehler, P. Edwards, M. Kappers, K. Lorenz, E. Alves, C. McAleese, C. Humphreys, and R. Martin, "Composition and luminescence studies of InGaN epilayers grown at different hydrogen flow rates," Semiconductor Science and Technology **28**, 065011 (2013).

[22]S. Rhode, W. Y. Fu, M. Moram, F. Massabuau, M. Kappers, C. McAleese, F. Oehler, C. Humphreys, R. Dusane, and S. Sahonta, "Effect of Defects on Strain-Relaxation in In$_x$Ga$_{1-x}$N Epilayers," Journal of Applied Physics **116**, 103513 (2014).

[23]F. Massabuau, S.-L. Sahonta, L. Trinh-Xuan, S. Rhode, T. Puchtler, M. Kappers, C. Humphreys, and R. Oliver, "Morphological, structural, and emission characterization of trench defects in InGaN/GaN quantum well structures," Applied Physics Letters **101**, 212107 (2012).

[24] J. Bruckbauer, P. Edwards, T. Wang, and R. Martin, "High resolution cathodoluminescence hyperspectral imaging of surface features in InGaN/GaN multiple quantum well structures," Applied Physics Letters **98**, 141908 (2011).

[25] V. Narayanan, K. Lorenz, W. Kim, and S. Mahajan, "Gallium nitride epitaxy on (0001) sapphire," Philosophical Magazine A **82**, 885 (2002).

[26] R. Oliver, M. Kappers, J. Sumner, R. Datta, and C. Humphreys, "Highlighting threading dislocations in MOVPE-grown GaN using an in situ treatment with SiH4 and NH3," Journal of Crystal Growth **289**, 506 (2006).

[27] S. Rhode, M. Horton, M. Kappers, S. Zhang, C. Humphreys, R. Dusane, S.-L. Sahonta, and M. Moram, "Mg Doping Affects Dislocation Core Structures in GaN," Physical Review Letters **111**, 025502 (2013).

[28] P. Edwards and R. Martin, "Cathodoluminescence and nano-characterization of semiconductors," Semiconductor Science and Technology **26**, 064005 (2011).

[29] K. Kanaya and S. Okayama, "Penetration and energy-loss theory of electrons in solid targets," J. Phys. D: Appl. Phys. **5**, 43 (1972).

[30] M. Toth and M. Phillips, "Monte Carlo Modeling of Cathodoluminescence Generation Using Electron Energy Loss Curves," Scanning **20**, 425 (1998).

[31] J. Muth, J. Lee, I. Shmagin, R. Kolbas, H. Casey, B. Keller, U. Mishra, and S. DenBaars, "Absorption coefficient, energy gap, exciton binding energy, and recombination lifetime of GaN obtained from transmission measurements," Applied Physics Letters **71**, 2572 (1997).

[32] D. Drouin, P. Hovington, and R. Gauvin, "CASINO: A new Monte Carlo code in C language for electron beam interactions - Part II: Tabulated values of the Mott cross section," Scanning **19**, 29 (1997).

[33] T. Smeeton, M. Kappers, J. Barnard, M. Vickers, and C. Humphreys, "Electron-beam-induced strain within InGaN quantum wells: False indium cluster detection in the transmission electron microscope," Applied Physics Letters **83**, 5419 (2003).

[34] K. Baloch, A. Johnston-Peck, K. Kisslinger, E. Stach, and S. Gradečak, "Revisiting the In-clustering question in InGaN through the use of aberration-corrected electron microscopy below the knock-on threshold," Applied Physics Letters **102**, 191910 (2013).

[35] S. Rhode, M. Horton, S. Sahonta, M. Kappers, S. Haigh, T. Pennycook, C. McAleese, C. Humphreys, R. Dusane, and M. Moram, "Dislocation core structures in (0001) InGaN," Journal of Applied Physics **119**, 105301 (2016).

[36]T. Song, "Strain relaxation due to V-pit formation in $In_xGa_{1-x}N$-GaN epilayers grown on sapphire," Journal of Applied Physics **98**, 084906 (2005).

[37]G. Orsal, Y. El Gmili, N. Fressengeas, J. Streque, R. Djerboub, T. Moudakir, S. Sundaram, A. Ougazzaden, and J. Salvestrini, "Bandgap energy bowing parameter of strained and relaxed InGaN layers," Optical Materials Express **4**, 1030 (2014).

[38]Q. Liu, J. Lu, Z. Gao, L. Lai, R. Qin, H. Li, J. Zhou, and G. Li, "Electron localization and emission mechanism in wurtzite (Al, In, Ga)N alloys," Physica Status Solidi (B) **247**, 109 (2010).

[39]S. Schulz, O. Marquardt, C. Coughlan, M. Caro, O. Brandt, and E. O'Reilly, "Atomistic description of wave function localization effects in In_{x} Ga_{1-x}N alloys and quantum wells," Proceedings of SPIE **9357**, 93570C (2015).

[40]S. Chichibu, A. Uedono, T. Onuma, B. Haskell, A. Chakraborty, T. Koyama, P. Fini, S. Keller, S. Denbaars, J. Speck, U. Mishra, S. Nakamura, S. Yamaguchi, S. Kamiyama, H. Amano, I. Akasaki, J. Han, and T. Sota, "Origin of defect-insensitive emission probability in in-containing (al,in,ga)n alloy semiconductors," Nature materials **5**, 810– (2006).

[41]M. Horton, S. Rhode, S.-L. Sahonta, M. Kappers, S. Haigh, T. Pennycook, C. Humphreys, R. Dusane, and M. Moram, "Segregation of In to Dislocations in InGaN," Nano letters **15**, 923 (2015).

[42]T. P. Peixoto, "The graph-tool python library," (2015).

[43]P. Hirsch, J. Lozano, S. Rhode, M. Horton, M. Moram, S. Zhang, M. Kappers, C. Humphreys, A. Yasuhara, E. Okunishi, and P. Nellist, "The dissociation of the [a + c] dislocation in GaN," Philosophical Magazine **93**, 3925 (2013).